Sensors and Materials, Vol. 37, No. 8 (2025) 3377–3387
MYU Tokyo

S & M 4123

Effect of an Electric-field-generating Grid on Sensor Output for Gases with Different Polarities

Manase Mizutani,[1,3] Naho Minowa,[1] Kaito Yotsugi,[1] Yong-Joon Choi,[1] Kazuhiro Takahashi,[1,2] Yoshihisa Suzuki,[3] Kazuaki Sawada,[1,2] and Toshihiko Noda[1,2*]

[1]Department of Electrical and Electronic Information Engineering, Toyohashi University of Technology, Toyohashi 441-8580, Japan
[2]Institute for Research on Next-generation Semiconductor and Sensing Science (IRES²), Toyohashi University of Technology, Toyohashi 441-8580, Japan
[3]Development Group, Sintokogio, Ltd., Toyokawa 442-8505, Japan

(Received February 14, 2025; accepted July 11, 2025)

Keywords: polarity, molecular structure, electric field, gas discrimination

Regarding gas sensors, in addition to diversifying detection methods, research is being conducted to improve the detection accuracy through machine learning. However, if the data quality is poor, machine learning does not lead to improved detection accuracy. However, one factor that can have an unexpected effect on gas sensor data is the presence of moisture in air. Gas molecules have an indicator of their affinity for water, called polarity. If the target gas is polar, it may be affected by water before it reaches the gas sensor, thereby causing the sensor output to change. However, if the target gas is not polar, it is less likely to be affected by water. We developed a grid that generates an electric field near the gas sensor. First, we verified whether we could obtain data that could be used for decision making using only the grid and sensor. We then improved the quality of the data so that they could be used for machine learning. In this study, we verified whether the gas sensor output differs between polar and nonpolar gas molecules depending on the strength of the electric field formed by the grid in the gas flow path. As a result, the gas sensor output for polar gases had a rounded waveform regardless of the effect of the grid. However, the gas sensor output waveform for nonpolar molecules was rectangular, regardless of the effect of the grid. In addition, the gas sensor outputs for the nonpolar and weakly polar molecules decreased while maintaining their respective waveforms. The results of this experiment suggest that the combination of a grid and a gas sensor may enable the identification of gases based on their polarity.

1. Introduction

Several researchers have investigated and developed gas sensors capable of detecting volatile organic compounds (VOCs) with high sensitivity. These sensors are widely used in the environmental field to detect vaporized solvents emitted by industries[(1)] and VOCs generated by the microbial decomposition of wastewater and garbage for odor control.[(2,3)] In healthcare, the

*Corresponding author: e-mail: noda.toshihiko.zk@tut.jp
https://doi.org/10.18494/SAM5602

ISSN 0914-4935
https://myukk.org/

detection of VOCs in exhaled and skin gases can be used to identify human diseases and illnesses.[4] In addition, research has been conducted using machine learning to detect low-concentration gases and achieve high selectivity in gas sensors.[5–7] In a recent study, Praveenchandar *et al.* proposed a device to prevent worker accidents caused by gas leaks, using multiple gas sensors and machine learning to analyze the sensor data.[8]

However, in the previous studies it has been found that the moisture present in air affects the gas sensor data. This issue is particularly important in situations where diluted gases must be detected under high-humidity conditions. The distortion of gas sensor data waveforms and changes in output values due to humidity have been extensively discussed in the literature.[4,9,10] One possible approach is to use machine learning to consider the conditions under which water molecules also arrive at the gas sensor when the gas to be detected arrives at the gas sensor.

We have proposed and validated slit-structured elements (grid) that sieve gas molecules before they reach the gas sensor.[11] These grids are designed to modify sensor characteristics by combining additional elements with the gas sensor. In addition, we measured the gas sensor output for ammonia at the same concentration, with and without the grid installed along the gas flow path, and found that installing the grid led to a decrease in the gas sensor output. Subsequently, an electric field was applied to the grid to allow the gas to pass through, and the output of the gas sensor for ammonia improved as the applied voltage increased.[12] Moreover, in a separate study, we observed different gas sensor outputs between three pairs of enantiomers.[13]

We assumed that the gas molecules were affected by the electric field, which caused changes in the output of the gas sensor. For example, we believe that the differences in the gas sensor outputs between enantiomers can be attributed to the ease with which their functional groups are ionized.[13] However, in addition to the target gas, numerous water molecules are present in air. Water molecules readily form bonds with other molecules, which can affect gas detectors and other gas molecules.

Molecules can have an electric charge, which indicates how much an electric field affects them [unit: C (Coulomb)]. Under these conditions, the molecules split into positively (δ^+) and negatively (δ^-) charged atoms. Molecules with both δ^+ and δ^- charges are polar molecules with an affinity for water. Polarity can also be quantified using the molecular dipole moment. The molecular dipole moment is a vector quantity that originates at δ^+ and points toward δ^-.[14] In a metal-oxide (MOx) gas sensor, the output changes when gas molecules bind to oxygen atoms in the detection area.[15,16] This change in output results from the formation of electrical bonds between the gas molecules and the oxide film on the surface of the gas sensor. In a previous study, the output was verified using the same concentration and gas sensor. The results showed that higher polarity leads to an increase in the output.[17] In contrast, nonpolar molecules are unlikely to enhance the gas sensor output.[4,18] Solomatin *et al.* found that when a gas sensor is covered with water molecules, bonding between the carbon atoms and the gas sensor is hindered, which impedes the gas sensor output from increasing.[19] Furthermore, non-polar molecules exhibit polarity owing to imbalances in the distribution of electrons and the positions of atomic nuclei under an electric field.[20]

The grid is expected to be used not dry (sufficiently moist). For example, in a 50% humidity or more) environment, the electric field generated by the grid can change the properties of the gas molecules, altering the gas sensor output, as shown in Fig. 1.

In this study, we aimed to obtain measurement data by subjecting gas sensor data to machine learning. Here, we assumed that the data would be used for machine learning and worked to obtain multiple pieces of data, including humidity, by using only the device in a controlled environment.

The magnitude of the polarity is considered an important parameter in investigating the trends of the sensor output. Therefore, the measurements were performed using three types of gas with similar structures but different polarity components.

Prior to the measurements, we performed a simulation to investigate the magnitude of the electric field strength between the aluminum wires of the grid and to consider how the electric field affects the gas. In the gas sensor output measurements, we collected time-series data on the gas sensor output and investigated the trends of the applied voltage and magnitude of the output.

2. Materials and Methods

2.1 Overview of sensing system

Figure 2 shows the jig used to fix the grid and the gas sensors in place. The grid was positioned directly above the gas sensor to ensure that the gas molecules were affected by the grid immediately before reaching the sensor. Voltage was applied to the grid using a power source, and the strength of the electric field around the grid was controlled by varying the applied voltage.

2.2 Simulations

Electric-field simulations were performed for each applied voltage to verify the strength of the electric field generated by the grid. The electromagnetic interface of COMSOL Multiphysics (version 6.0) was used for finite element calculations to simulate the electric field intensity around the grid. First, a steady-state solver was selected, and rectangular port boundary

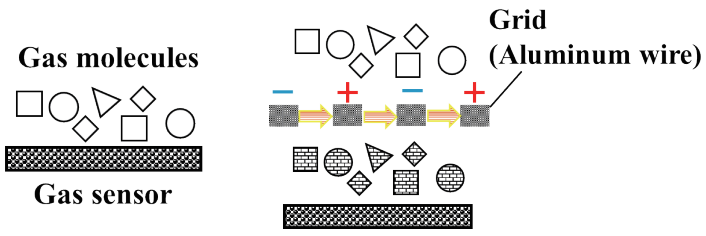

Fig. 1. (Color online) Expected effect of placing a grid in front of the gas sensor. (a) Without the grid. (b) With the grid.

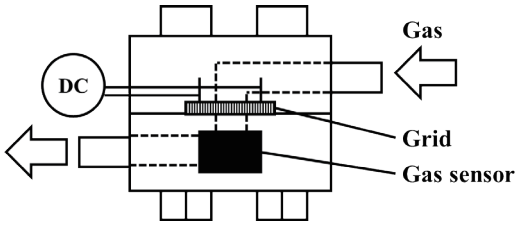

Fig. 2. Cross-sectional view of the gas sensing system with the grid.

conditions were used for the input ports. The relationship between the gas flow and the aluminum wires is shown in Fig. 3. In addition, the positive and negative electrodes were alternately connected to aluminum wires. The simulation results (Fig. 4) showed nine rectangles representing the cross section of the aluminum wire, with a short side of 1 μm and a long side of 15 μm. The cross sections of the aluminum wires were connected longitudinally at intervals of 15 μm, forming eight gaps. The color scale indicates the electric field strength, with red representing higher strength and blue denoting lower strength.

Figure 4 shows that the highest electric field is calculated at the boundary of the short side. The electric field strength decreased toward the midpoint of the gap, reaching its minimum value near this point. In the cross sections of the nine aluminum wires, neither end formed gaps with adjacent aluminum wires. These short sides, which did not form gaps, resulted in a lower electric field than the sides that formed the gaps. As shown in Fig. 4, the experimental results were analyzed considering the electric fields.

2.3 Experimental samples

Three gases with different polarities (acetone, isopropanol (IPA), and propane) were used to measure the gas sensor output. The structural formulae are shown in Fig. 5. These gases exhibit oxidizing and reducing relationships and share similar molecular structures. Water vapor was present in the experimental system during gas sensor measurements. The molecular dipole moment is expressed in Debye (D; 1 D = 3.336×10^{-30} C·m).[14] The dipole moments of the selected gases are approximately 2.93 D for acetone vapor,[21] 1.66 D for IPA vapor,[22] and 0.08 D for propane.[23] In addition, the dipole moment of water vapor is approximately 1.85 D.[24,25] Other major components in the air, such as nitrogen, oxygen, and carbon dioxide, have dipole moments of 0 D.

Acetone and IPA vapors were prepared using acetone (Product Code: 016-00346) and IPA (Product Code: 166-04836) from FUJIFILM Wako Pure Chemical Corporation, respectively. Because both are liquids, we used a permeator (PD-1B, GASTEC CORPORATION) to generate gases for the experiments. For each vapor, 2 mL of the respective solution was placed in a diffusion tube (D-10, GASTEC CORPORATION). The diffusion tube was placed in a permeator at 40 °C. The flow rate of the nitrogen gas for dilution was set to 0.5 L/min. Diluted gases were generated in this manner with the respective concentrations of acetone (100 ppm) and IPA (10 ppm). Subsequently, 50 mL of acetone vapor and 500 mL of IPA vapor were collected using a syringe and diluted with nitrogen gas to obtain a 10 L sample with a concentration of 0.5 ppm. In

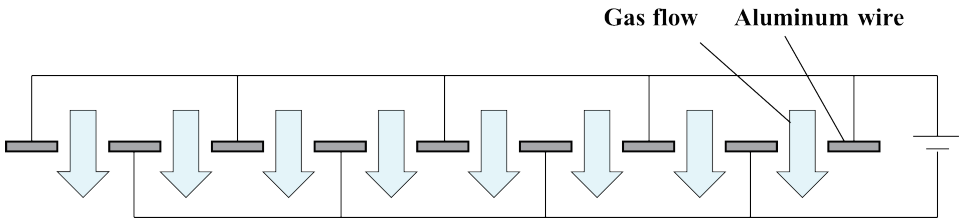

Fig. 3. (Color online) Schematic of gas flow and aluminum wires with applied voltage.

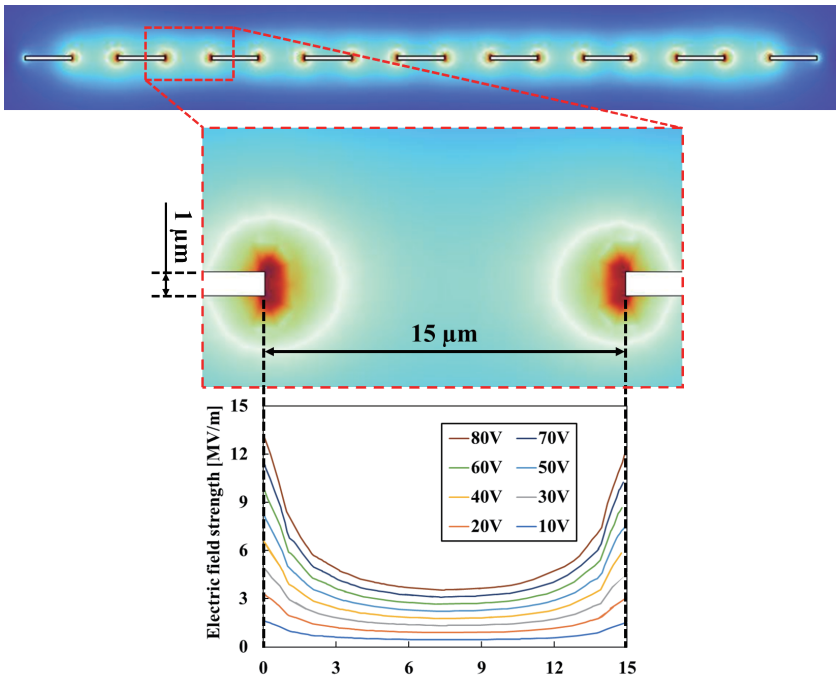

Fig. 4. (Color online) Simulation of the electric field strength between aluminum wires.

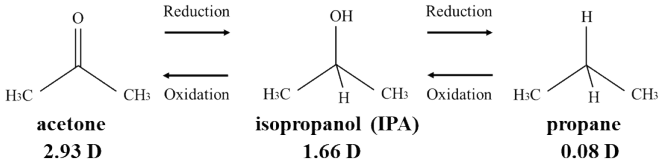

Fig. 5. Molecular structures and dipole moments of the three components (acetone, IPA, and propane) and water.

addition, 3 L of propane standard gas (GL Sciences; Cat. No. 1020-11005) was used. Five microliters of this sample was collected using a syringe and placed in a 10 L sampling bag. Propane was then diluted to 0.5 ppm with nitrogen gas.

2.4 Experimental method

In this study, we fabricated and used the same grid that had been proven to be effective in confirming changes in gas sensor output in previous study.[13] Figure 6 shows the front [Fig. 6(a)] and back [Fig. 6(b)] of the printed circuit board (PCB). The grid was fabricated by forming an aluminum wire pattern on a silicon substrate using MEMS processing and then affixed to the PCB using an epoxy adhesive. The grid contained 36 through-holes evenly spaced in both the x- and y-directions within a 300 μm × 300 μm area. In addition, aluminum wires were placed on top of the through-holes. The aluminum wires were approximately 1 μm thick and 15 μm wide with a line-and-space of 15 μm. The grid was mounted on a PCB (Q048; DAISEN Electronics Industrial Co.. Ltd.) measuring 1 × 1 cm^2, with a φ6 hole drilled in the center. The aluminum wires were then connected to the PCB electrode via wire bonding. When voltage was applied to the PCB electrode, an electric field was generated around the aluminum wire.

Figures 7(a) and 7(b) show photographs of the jig before and after assembly. The PCB was positioned between the top and bottom parts and secured with four bolts and nuts to complete the assembly. As shown in Fig. 7(b), gas entered through the side wall of the top part, passed through a φ6 hole in the PCB, and exited through the side wall of the bottom part. The bottom part contained a hole for inserting the gas sensor. After the gas sensor was inserted, adhesive rubber was used as a seal to prevent gas leakage. The grid was positioned at approximately 8 mm above the gas sensor. Figure 7(c) shows the overhead view of the assembled jig. The top part had

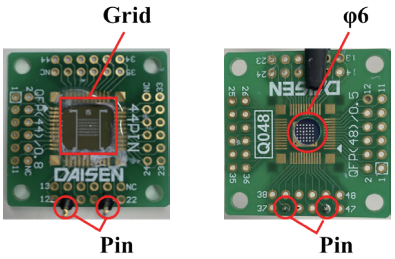

Fig. 6. (Color online) Photographs of the grid fixed onto the PCB: (a) front side and (b) back side.

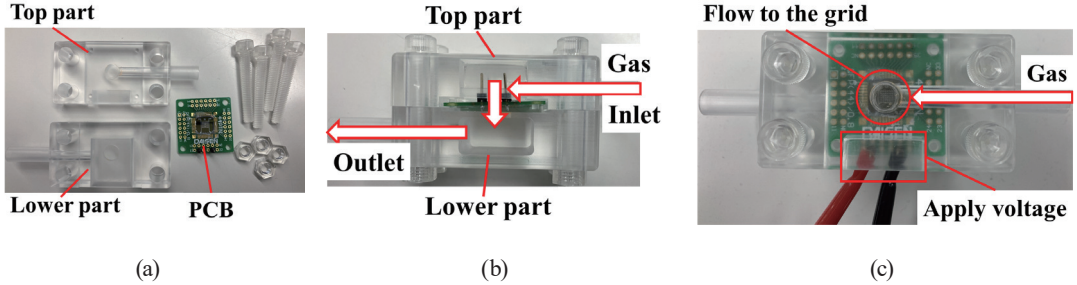

Fig. 7. (Color online) (a) Parts of the jig (before assembly). (b) Side and (c) overhead views of the assembled jig.

space to connect the PCB electrodes to the power supply. As shown in Fig. 7, the jig was transparent, allowing for easy observation of the interior. During the experiment, the jig prevented external light from penetrating the grid or the gas sensor. The jig, bolts, and nuts were composed of polycarbonates.

We used a semiconductor gas sensor (CCS-811, ams-OSRAM AG) that detects gases through changes in conductivity.[26] Metal oxide (MOx) is used as the material for the gas detection section.

Owing to the interaction of gas molecules with the MOx surface, the internal electrical carrier concentration will be affected. The resulting change in resistance can be used as the output of the gas sensor to measure the concentration of the target gas. The concentration output of the gas sensor was expressed as the equivalent total volatile organic compounds (eTVOC). eTVOC is an index unique to the gas sensor CCS-811 used in this study. It represents the total volatile organic compound concentration in an indoor environment. Depending on the type of volatile organic compound, the output may be higher or lower than the total volatile organic compound concentration (TVOC), which is often used as the output value of VOC gas sensors. In addition, the data sheet indicates that the sensitivity of eTVOC may decrease if the sensor is operated constantly in a high-temperature, high-humidity environment. The gas sensor was connected to a microcontroller unit (MCU), and the eTVOC was outputted by an analog-to-digital converter built into the MCU. The temperature and relative humidity of the gas were measured using a capacitive temperature and humidity sensor (SHT30-DIS, Sensirion AG).[27] CCS-811 and SHT30-DIS are on the same board and can acquire data simultaneously. Bags containing the prepared sample gases and N_2 were permeable to atmospheric moisture. Before the measurements, the gas in the bag was exposed to the SHT30-DIS, and the humidity of the gas was measured. At this time, the humidity was increased to 50±10%, and the experiment was conducted after the humidity had settled to a certain level.

The grid and gas sensor were initially exposed to N_2 for a duration of 100 seconds, followed by exposure to the sample gas for another 100 s, and subsequently returned to N_2 exposure for an additional 100 s. The output from the gas sensor was recorded at intervals of every 5 s.. The voltage applied to the grid was increased from 0 to 80 V in increments of 10 V. Each voltage condition was repeated thrice, and the average value was recorded. The data used to create the graph were as follows. First, during measurements at 0 V, eight consecutive readings were taken to ensure that the output did not increase owing to sensor warming and other factors. As shown in Fig. 8, the average values of the 6th to 8th measurements were used at 0 V. When 10–80 V was applied, measurements were performed four consecutive times, and the average values of the 2nd to 4th measurements were used.

2.5 Experimental results

Figure 8 shows the experimental results for each gas. Figures 8(a)–8(c) show the time-series data for acetone, IPA, and propane, respectively. In these graphs, the eTVOC every 5 s was normalized to the eTVOC at 190 s at 0 V. Figure 8(d) shows the standard values of the output over 190 s at each applied voltage, with the output measured at 0 V for 190 s considered as 1. The

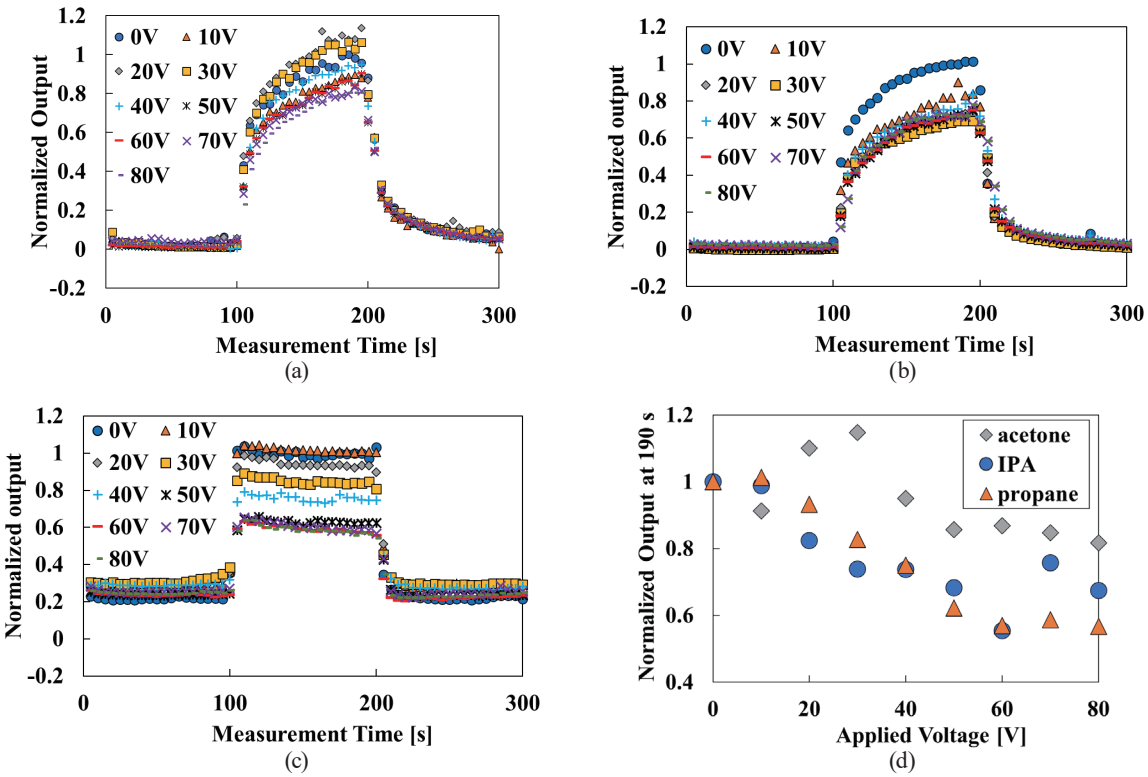

Fig. 8. Time-series data for (a) acetone, (b) IPA, and (c) propane gas detection at each voltage applied to the grid. (d) Plots of 190 s of time-series data for each applied voltage.

time-series data in Figs. 8(a)–8(c) exhibit scattering attributable to fluctuations in the output; however, the trend becomes clearer in Fig. 8(d).

As shown in Figs. 8(a) and 8(d), when 10 V was applied to the grid, the output of acetone decreased compared with that at 0 V. However, after applying 20 and 30 V to the grid, the output increased compared with that at 0 V, reaching its maximum value at 30 V. When a voltage of 40 V or higher is applied to the grid, the output decreases below the level observed at 0 V. When 80 V was applied to the grid, the output was 0.82 compared with that at 0 V. In contrast, as shown in Fig. 8(b), when voltage was applied to the grid in the case of IPA vapor, the output was significantly lower than that at 0 V. However, as shown in Fig. 8(d), when the voltage applied to the grid was 30 V or more, the output of IPA ranged between 0.67 and 0.75, except at 60 V.

Figure 8(c) shows that the waveform of the time-series data for propane differs from those of acetone and IPA. At 100 s, when the gas was introduced, the output increased abruptly and then decreased gradually, until the gas was switched to N_2 at 200 s. In addition, even after switching from propane to N_2, the output did not return to 0, but remained between 0.2 and 0.3. In the case of propane [Fig. 8(d)], as the voltage applied to the grid increased from 10 to 60 V in increments of 10 V, the coefficient of resistance decreased linearly from 1 to 0.57.

3. Discussion

The change in the gas sensor output according to the magnitude of the voltage applied to the grid was determined to be due to the formation of bonds between gas molecules in the electric field or the loss of gas molecules due to discharge occurring between the grids.

The output of the acetone gas sensor was higher only when voltages of 20 and 30 V were applied, compared with when no voltage was applied. We attribute this result to the electric field causing a significant imbalance in the charge within the molecule, that is, an increase in the molecular dipole moment. We also believe that this increased the energy during the gas sensor adsorption, which led to an increased output.

For all three types of gas, the output tended to decrease as the voltage applied to the grid increased. One possible reason for this phenomenon is that when gas passes through an electric field, the target gas and water molecules become charged before reaching the gas sensor, making them more likely to form hydrogen bonds with each other. This suggests that as the bonds between the gases become stronger, it becomes more difficult for the gas molecules to be adsorbed onto the gas sensor.

We also investigated the possibility of discharge between the aluminum wires using simulations. Unlike the static effect of an electric field, discharge between aluminum wires instantaneously applies a substantial amount of energy to the gas molecules. When discharge occurs, gas molecules either transform or disappear. The electric field strength at which discharge occurs in the atmosphere is 3 MV/m.[28] However, the electric field strength required for discharge changes when the gap is narrow. The electric field strength required for discharge in a 15 μm gap is approximately 50 MV/m, which corresponds to a voltage of 600 V or more.[29–31] In this study, the maximum applied voltage was 80 V, resulting in a maximum electric field of 13 MV/m. Therefore, discharge did not occur when the voltage was applied to the grid, and the high energy generated by the discharge was not locally applied to the gas molecules.

To distinguish three components with similar structures based on the data, the shapes of the time-series data can first be compared between polar (acetone and IPA) and nonpolar molecules (propane). Consequently, both IPA and propane were found to exhibit increased polarity depending on the electric field strength, and the output decreased accordingly. The results of this experiment show that the gas sensor output can be distinguished on the basis of the magnitude of polarity using a grid.

In our previous study, three pairs of enantiomers were used to assess whether differences in the gas sensor output occurred depending on the voltage applied to the grid.[13] In this case, one of the gas sensor outputs did not change significantly from 0 to 80 V, whereas the outputs of the other sensors increased with the applied voltage. In other words, the gas sensor output did not decrease with increasing applied voltage. We believe that this result can be attributed to the large molecular weights of the gas components used, which weakened the observed effect.

In this study, by applying a voltage to the grid, data showing different waveforms and increasing and decreasing trends were obtained from three components with similar structures (acetone, IPA, and propane). With such differences, it is expected that these data will be useful for machine learning.

4. Conclusions

In this study, a grid was used to investigate whether the output of the gas sensor changed depending on the magnitude of the polarity. Three components with different polarities but similar chemical compositions and molecular structures (acetone, IPA, and propane) were used as the target gases. We also simulated the electric field strength between the aluminum wires of the grid to investigate whether the field would be sufficiently strong to cause the gas molecules to disappear.

After exposing the gas sensor to polar acetone and IPA gases, the gas sensor output gradually increased and the graph became rounded. Differences were observed in the decreasing trend of the gas sensor output with increasing applied voltage. In the experimental results, the output of acetone increased at the applied voltages of 20 and 30 V. In contrast, propane, a nonpolar molecule, exhibited a steep rise in the square wave. In addition, the decreasing trend of the gas sensor output with increasing applied voltage was similar to that of the IPA gas. These results suggest that it may be possible to distinguish gases on the basis of their size, even among polar molecules.

Although voltages of up to 80 V were applied to the grid, simulations confirmed that the electric field strength was insufficient to cause a discharge; therefore, the gas molecules would not have disappeared or gained significant energy. However, more detailed data must be collected, and the relationship between the electric field of the grid and the output of the gas sensor, as well as the phenomena occurring between gas molecules, must be fully considered.

In this experiment, a dataset was obtained in which the trends of each component differed depending on the combination of the grid and gas sensor. However, in practical applications, it is expected that the grid can be used in situations where gases with similar polarities are mixed. In the future, we plan to conduct measurements in situations where mixed gases are present and to expand the diversity of the data.

Acknowledgments

This work was supported by MEXT Initiative to Establish Next-generation Novel Integrated Circuits Centers (X-NICS) Grant Number JPJ011438, JST OPERA Grant Number JPMJOP1834, and KAKENHI Grant Numbers JP21K18718 and JP24K21610, Japan.

References

1 B. Khaniyev, M. Ibraimov, Y. Sagidolda, Y. Tezekbay, T. Duisebayev, A. Tileu, and A. Khaniyeva: Coatings **13** (2023) 190. https://doi.org/10.3390/coatings13010190
2 D. González, D. Gabriel, and A. Sánchez: Atmosphere **13** (2022) 798. https://doi.org/10.3390/atmos13050798
3 J. Hou, C. Yu, F. Meng, X. He, Y. Wang, W. Chen, and M. Li, RSC Advances **11** (2021) 39924. https://doi.org/10.1039/D1RA05962A
4 A. Sachan, M. Castro, V. Choudhary, and J.-F. Feller: Chemosensors **6** (2018) 64. https://doi.org/10.3390/chemosensors6040064
5 S. Lu, J. Guo, S. Liu, B. Yang, M. Liu, L. Yin, and W. Zheng: Appl. Sci. **12** (2022) 9529. https://doi.org/10.3390/app12199529

6 T. Nakamoto, N. Cho, N. Nitikarn, B. Wyszynski, H. Takushima, and M. Kinoshita: Proc. 18th Int. Conf. Artificial Reality and Telexistence (2008) 1–4.
7 S. Kuroda, Y. Nakaya, K. Tatematsu, and S. Hinuma: Sensors **23** (2023) 6164. https://doi.org/10.3390/s23136164
8 J. Praveenchandar, D. Vetrithangam, S. Kaliappan, M. Karthick, N. K. Pegada, P. P. Patil, S. G. Rao, and S. Umar: Sci. Program **2022** (2022) 7516328. https://doi.org/10.1155/2022/7516328
9 D.-W. Liao, A. M. Mebel, Y.-T. Chen, and S.-H. Lin: J. Phys. Chem. A **101** (1997) 9925. https://doi.org/10.1021/jp972102q
10 Z. Liu, T. Yang, Y. Dong, and X. Wang: Sensors **18** (2018) 3113. https://doi.org/10.3390/s18093113
11 R. Wada, N. Minowa, T. Wada, M. Mizutani, Y. Suzuki, Y.-J. Choi, K. Takahashi, K. Sawada, and T. Noda: Proc. IEEE Sensors (2021) 1–4.
12 N. Minowa, M. Mizutani, Y. Suzuki, Y.-J. Choi, K. Takahashi, K. Sawada, and T. Noda: Proc. 22nd Int. Conf. Solid-State Sensors, Actuators, and Microsystems (Transducers) (2023) 1157–1160.
13 M. Mizutani, N. Minowa, Y.-J. Choi, K. Takahashi, Y. Suzuki, K. Sawada, and T. Noda: Sens. Mater. **37** (2025) 4. https://doi.org/10.18494/SAM5304
14 A. Kuwano, K. Nittoh, T. Ikehara, T. Yoshida, I. Yoguchi, T. Watanabe, and K. Suzuki: J. Nucl. Sci. Technol. **34** (1997) 360. https://doi.org/10.1080/18811248.1997.9733675
15 Z. Li, H. Li, Z. Wu, M. Wang, J. Luo, H. Torun, P. Hu, C. Yang, M. Grundmann, X. Liu, and Y. Fu: Mater. Horiz. **6** (2019) 470. https://doi.org/10.1039/C8MH01365A
16 M. V. Nikolic, V. Milovanovic, Z. Z. Vasiljevic, and Z. Stamenkovic: Sensors **20** (2020) 6694. https://doi.org/10.3390/s20226694
17 S. Neogi and R. Ghosh: Sens. Actuators B: Chem. **415** (2024) 135980. https://doi.org/10.1016/j.snb.2024.135980
18 M. Zhang, S. Inoue, and Y. Matsumura: RSC Adv. **14** (2024) 24985. https://doi.org/10.1039/D4RA04474F
19 M. A. Solomatin, O. E. Glukhova, F. S. Fedorov, M. Sommer, V. V. Shunaev, A. S. Varezhnikov, A. G. Nasibulin, N. M. Ushakov, and V. V. Sysoev: Chemosensors **9** (2021) 181. https://doi.org/10.3390/chemosensors9070181
20 P. Atkins, J. de Paula, and J. Keeler: Atkins' Physical Chemistry (Oxford University Press, Oxford, 2006) pp. 1, 18, 620–623.
21 O. Dorosh and Z. Kisiel: Acta Phys. Pol. A **112** (2007) S95. https://doi.org/10.12693/APhysPolA.112.S-95
22 M. Jorge, J. R. B. Gomes, and M. C. Barrera: J. Mol. Liq. **356** (2022) 119033. https://doi.org/10.1016/j.molliq.2022.119033
23 M. H. F. Bettega, R. F. da Costa, and M. A. P. Lima: Phys. Rev. A **77** (2008) 052706. https://doi.org/10.1103/PhysRevA.77.0527066
24 D. D. Kemp and M. S. Gordon: J. Phys. Chem. A **112** (2008) 4885. https://doi.org/10.1021/jp801921f
25 Y. Tu and A. Laaksonen: Chem. Phys. Lett. **329** (2000) 283. https://doi.org/10.1016/S0009-2614(00)01026-5
26 ams-OSRAM AG, CCS811 Datasheet. https://cdn.sparkfun.com/assets/2/c/c/6/5/CN04-2019_attachment_CCS811_Datasheet_v1-06.pdf (accessed January 2024).
27 Sensirion AG, SHT3x-DIS Datasheet. https://sensirion.com/media/documents/213E6A3B/63A5A569/Datasheet_SHT3x_DIS.pdf (accessed June 2025).
28 A. Krupa: J. Phys. Conf. Ser. **301** (2011) 012022. https://doi.org/10.1088/1742-6596/301/1/012022
29 G. Meng, X. Gao, A. M. Loveless, C. Dong, D. Zhang, K. Wang, B. Zhu, Y. Cheng, and A. L. Garner: Phys. Plasmas **25** (2018) 082116. https://doi.org/10.1063/1.5046335
30 A. M. Loveless, G. Meng, Q. Ying, F. Wu, K. Wang, Y. Cheng, and A. L. Garner: Sci. Rep. **9** (2019) 5669. https://doi.org/10.1038/s41598-019-42111-2
31 G. Meng and Y. Cheng: Electrostatic Discharge: From Electrical Breakdown in Micro-gaps to Nano-generators (IntechOpen, London, 2019) p. 29. https://doi.org/10.5772/intechopen.86915